Astronomy & Astrophysics

The largest metallicity difference in twin systems: High-precision abundance analysis of the benchmark pair Krios and Kronos

P. Miquelarena[1,2,6], C. Saffe[1,2,6], M. Flores[1,2,6], R. Petrucci[5,6], J. Yana Galarza[7], J. Alacoria[1,6],
M. Jaque Arancibia[3,4], E. Jofré[5,6], K. Montenegro Armijo[8], and F. Gunella[1,6]

[1] Instituto de Ciencias Astronómicas, de la Tierra y del Espacio (ICATE-CONICET), C.C 467, 5400, San Juan, Argentina
e-mail: paulamique@gmail.com
[2] Universidad Nacional de San Juan (UNSJ), Facultad de Ciencias Exactas, Físicas y Naturales (FCEFN), San Juan, Argentina
[3] Instituto de Investigación Multidisciplinar en Ciencia y Tecnología, Universidad de La Serena, Raúl Bitrán 1305,
La Serena, Chile
[4] Departamento de Astronomía, Universidad de La Serena, 1305, La Serena, Chile
[5] Universidad Nacional de Córdoba, Observatorio Astronómico de Córdoba, Laprida 854, Córdoba X5000BGR, Argentina
[6] Consejo Nacional de Investigaciones Científicas y Técnicas (CONICET), Buenos Aires, Argentina
[7] The Observatories of the Carnegie Institution for Science, 813 Santa Barbara Street, Pasadena, CA 91101, USA
[8] Clínica Universidad de los Andes, Dirección Comercial, Chile

ABSTRACT

Aims. We conducted a high-precision differential abundance analysis of the remarkable binary system HD 240429/30 (Krios and Kronos, respectively), whose difference in metallicity is one of the highest detected to date in systems with similar components ($\sim$0.20 dex). A condensation temperature T_C trend study was performed to search for possible chemical signatures of planet formation. In addition, other potential scenarios are proposed to explain this disparity.

Methods. Fundamental atmospheric parameters (T_{eff}, log g, [Fe/H], v_{turb}) were calculated using the latest version of the FUNDPAR code in conjunction with ATLAS12 model atmospheres and the MOOG code, considering the Sun and then Kronos as references, employing high-resolution MAROON-X spectra. We applied a full line-by-line differential technique to measure the abundances of 26 elements in both stars with equivalent widths and spectral synthesis taking advantage of the non-solar-scaled opacities to achieve the highest precision.

Results. We find a difference in metallicity of $\sim$0.230 dex: Kronos is more metal rich than Krios. This result denotes a challenge for the chemical tagging method. The analysis encompassed the examination of the diffusion effect and primordial chemical differences, concluding that the observed chemical discrepancies in the binary system cannot be solely attributed to any of these processes. The results also show a noticeable excess of Li of approximately 0.56 dex in Kronos, and an enhancement of refractories with respect to Krios. A photometric study with TESS data was carried out, without finding any signal of possible transiting planets around the stars. Several potential planet formation scenarios were also explored to account for the observed excess in both metallicity and lithium in Kronos; none was definitively excluded. While planetary engulfment is a plausible explanation, considering the ingestion of an exceptionally high mass, approximately $\sim$27.8 $M_\oplus$, no scenario is definitively ruled out. We emphasize the need for further investigations and refinements in modelling; indispensable for a comprehensive understanding of the intricate dynamics within the Krios and Kronos binary system.

Key words. stars: abundances – binaries: general – planetary systems

1. Introduction

The chemical tagging technique consists in the possibility of identifying co-natal stars that have dispersed into the Galactic disc based on chemistry alone (e.g. Freeman & Bland-Hawthorn 2002; Casamiquela et al. 2021). This idea has been one of the motivations of important surveys such as APOGEE, GALAH, and the *Gaia*-ESO survey (Gilmore et al. 2012; Randich et al. 2013; De Silva et al. 2015; Majewski et al. 2017). A fundamental assumption guiding these surveys is that the members of the birth cluster should exhibit a chemically homogeneous composition. This hypothesis was tested using main-sequence and red giant stars in open clusters, reaching an internal coherence in metallicity in the range 0.02–0.03 dex (e.g. De Silva et al. 2006; Bovy 2016; Liu et al. 2016; Casamiquela et al. 2020, 2021). Originally proposed by Andrews et al. (2018), wide binaries (100 au < a < 1 pc) are an ideal sample for studying

chemical tagging (e.g. Andrews et al. 2019; Kamdar et al. 2019a; Hawkins et al. 2020). In particular, for the case of binaries with physically similar components, it is possible to reach the highest possible precision through a line-by-line differential analysis (e.g. Schuler et al. 2011; Saffe et al. 2015, 2017; Teske et al. 2016; Liu et al. 2018; Tucci Maia et al. 2019; Jofré et al. 2021; Flores et al. 2024), which helps to minimize a number of model-induced and other systematic errors (see Nissen & Gustafsson 2018).

Recently, the internal coherence of the chemical tagging was strongly challenged by the discovery of the exceptional comoving pair HD 240429/30 (hereafter Krios and Kronos; Oh et al. 2018), composed of two G-type stars sharing nearly identical *Gaia* TGAS[1] proper motions and parallaxes. Oh et al. (2018) suggest that the two stars are co-natal, based on their proximity

---

[1] The Tycho-*Gaia* Astrometric Solution catalogue (TGAS) is a component of *Gaia* DR1 (Michalik et al. 2015).

in phase-space, with very similar radial velocities and isochrone ages, and also with very low probabilities of stellar capture and exchange scattering. The authors used the stellar parameters and abundances from the survey of Brewer et al. (2016), who studied 1617 FGK stars that belong to the California Planet Survey (CPS) using an automated spectral synthesis procedure. In this way, Oh et al. (2018) estimated for the pair a mutual difference in iron content of ~0.20 dex, and a similar value for other metals such as Ca and Ni. To our knowledge, this is the largest difference found to date between stars with twin components and a supposed common origin, highlighting the pair Kronos and Krios as a benchmark multiple system.

Hawkins et al. (2020) studied 25 binary systems and found that 80% are homogeneous at the 0.02 dex level, while six pairs show differences greater than 0.05 dex. Then, if confirmed, the metallicity difference between Kronos and Krios would be ten times higher, in logaritmic scale, than the typical internal coherence of stars born in the same cluster. The greatest difference found between Kronos and Krios would imply that their co-natal nature could not be recovered by any previous chemical tagging work (e.g. De Silva et al. 2006; Bovy 2016; Liu et al. 2016; Casamiquela et al. 2020, 2021). The difference between Kronos and Krios (~0.2 dex) is similar to those found between random pairs (scatter of 0.23 dex, Nelson et al. 2021), defying the main assumption of the chemical tagging, in which stars formed together display the same abundances along their main sequence lifetimes. Recently, Saffe et al. (2024) analysed, for the first time, a giant–giant binary system bringing new insights, with significant differences in metallicity potentially attributed to primordial inhomogeneities. The significance of these findings underscores the importance of our binary system and deserves particular attention.

In addition, it is equally important to explain the origin of the significant metallicity difference between Kronos and Krios. This requires studying the relative volatile-to-refractory content between the stars and the condensation temperature (T_c) trends. For instance, Meléndez et al. (2009) found that the Sun is deficient in refractory elements ($T_c > 900$ K) relative to volatile ($T_c < 900$ K) when compared to 11 solar twins, and that the abundance differences correlate with T_c. They suggested that this trend is a signature of planet formation, assuming that refractory elements were locked up in rocky planets during the Solar System formation. However, different explanations for the T_c trends could also be possible. Booth & Owen (2020) suggest that if a giant planet forms early enough (≲1 Myr) at large separations, it could trap ≳100 $M_\oplus$ of dust exterior to its orbit. Then, the star would accrete more gas than dust from the protoplanetary disc, which could result in a lack of refractories in the stellar atmosphere. A larger amount of refractories in a stellar atmosphere could also be the result of accretion of rocky material (e.g. Gonzalez 1997; Meléndez et al. 2017; Saffe et al. 2017; Oh et al. 2018). Oh et al. (2018) suggested that Kronos accreted ~15 $M_\oplus$ of rocky material in order to explain the mutual T_c trend. To date, this is the highest amount of material estimated to be accreted in binary systems with twin components: it is equivalent to approximately seven times the four inner planets of the Solar System together, which is also remarkable. Other authors consider alternative scenarios trying to explain the T_c trends, such as Galactic chemical evolution (GCE) or dust-cleansing effects (e.g. Önehag et al. 2011; Adibekyan et al. 2014; Nissen 2015).

Recently, Spina et al. (2021) studied a sample of 107 binary systems and showed that accretion events occur in ~20–35% of solar-type stars. In contrast, Behmard et al. (2023) found a much lower engulfment rate of ~2.9%, claiming that accretion events are rarely detected. The last authors propose that primordial inhomogeneities rather than engulfment events could explain the differences observed in binary systems. According to their criteria (see Sect. 6), Kronos and Krios would be the only pair showing a true engulfment detection, ruling out most previous claims of engulfment events. This highlights again the relevance of the notable pair Kronos and Krios between other binary systems. Interestingly, Kunimoto et al. (2018) consider an engulfment event unlikely in this binary system, owing to the rapid mixing expected from fingering convection (10–100 Myr, Théado & Vauclair 2012). Thus, the origin of the extreme metallicity difference in this benchmark pair remains unknown.

A number of recent works studied atomic diffusion effects on main-sequence stars, using stellar evolution models (e.g. Dotter et al. 2017), observing the stars of the M67 open cluster (e.g. Souto et al. 2018, 2019) and also using binary stars (e.g. Ramírez et al. 2019; Liu et al. 2021). Diffusion models show a strong dependence on log g, with the largest effects occurring near log $g \sim 4.2$ dex (see e.g. Fig. 5 in Souto et al. 2019). The same plot predicts that a difference of ~0.20 in log g could translate into a difference of ~0.075 in [Fe/H]; other differences are predicted for different chemical elements. Liu et al. (2021) found that the overall abundance offsets in four of seven binary systems could be due to atomic diffusion effects, complicating the chemical tagging. The difference in log g estimated for the pair Kronos–Krios is 0.10 dex (Brewer et al. 2016), the largest difference found in the sample of twin-star binary systems of Ramírez et al. (2019). Then, we wondered if atomic diffusion effects not previously studied in this benchmark pair could explain, at least in part, the extreme difference in metallicity found.

The detection of a possible T_c trend in a binary or multiple system is a challenge, requiring the highest possible precision in the derivation of stellar parameters and abundances. This demands high-quality spectra with very high S/N, reaching typically ~400 or even more (e.g. Teske et al. 2016; Liu et al. 2018; Schuler et al. 2011; Tucci Maia et al. 2019), compared to $S/N \sim 200$ for the case of Kronos and Krios (Oh et al. 2018). For stars with low rotational velocities, it is usual to use equivalent widths rather than spectral synthesis in the derivation of stellar parameters, given that spectral synthesis depends on additional factors (such as $v \sin i$, the resolving power R of the instrument, and the correct fitting of line profiles). The stars Kronos and Krios present projected rotational velocities of 1.1 km s^{-1} and 2.5 km s^{-1} (Brewer et al. 2016), allowing a clean measurement of equivalent widths. Moreover, for the case of multiple systems with physically similar components, the use of a line-by-line differential technique allows the minimization of systematic errors (e.g. Schuler et al. 2011; Bedell et al. 2014; Saffe et al. 2015; Teske et al. 2016; Liu et al. 2018; Tucci Maia et al. 2019). In this way, the physical similarity between Kronos and Krios (G0V+G2V) is an advantage to be exploited with a differential analysis, a technique not applied by previous works for this pair.

Then we studied the benchmark pair Kronos and Krios by using a high-quality MAROON-X spectra with higher S/N (~400), higher resolving power ($R \sim 85\,000$), broader spectral coverage (from ~4900 to 9200 Å), and using a more refined analysis technique than previous works (fully differential together with equivalent widths). In addition, we took advantage of using non-solar-scaled opacities in the derivation of model atmospheres, which could result in small abundance differences when compared to the classical solar-scaled methods (Saffe et al. 2018, 2019; Flores et al. 2024). This allowed us to determine a metallicity difference between the two stars with the highest possible

precision, and to perform a T_c trend analysis to study the possible origin of the differences in this benchmark pair, which could be attributed to a planet engulfment event (Oh et al. 2018; Behmard et al. 2023). Moreover, we explored alternative scenarios that could lead to this result, such as atomic diffusion (Liu et al. 2021) and the potential primordial origin of the chemical difference (Ramírez et al. 2019; Nelson et al. 2021; Saffe et al. 2024).

This work is organized as follows. In Sect. 2, we describe the observations and data reduction. In Sect. 3, we present the stellar parameters and chemical abundance analysis. In Sect. 4, we show the results and discussion. Finally, in Sect. 5 we highlight our main conclusions.

2. Observations and data reduction

The spectra of Kronos and Krios were acquired through the M-dwarf Advanced Radial velocity Observer Of Neighboring eXoplanets (MAROON-X) spectrograph[2]. This high-precision bench-mounted echelle spectrograph provides high-resolution ($R \sim 85\,000$) spectra when illuminated via two 100 μm (0.″77 on sky) octogonal fibres. MAROON-X is connected to the 8.1 m Gemini North telescope at Maunakea, Hawaii. Currently, the spectrograph has no movable parts and is operated in one read-out mode (100 kHz, 1×1 binning). MAROON-X is equiped with two STA4850 (4080×4080) CCD detectors with a pixel size of 15 μm, including a coating optimized for their respective wavelength coverage. The instrument includes its own tungsten-halogen lamp for flat-fielding and a ThAr arc lamp for wavelength calibration.

The observations were taken on August 15, 2022 (Programme ID: GN-2022B-Q-203, PI: Paula Miquelarena); the star Kronos was observed immediately after the star Krios, using the same spectrograph configuration. The exposure times for Krios and Kronos were 3×20 min and 3×16.67 min, respectively. This resulted in a final signal-to-noise ratio (S/N) per pixel of ~420 for both stars, measured near ~6000 Å in the combined spectra. The final spectral coverage was ~4900–9200 Å. The solar spectrum was obtained by observing the asteroid Vesta (Programme ID: GN-2022A-Q-22, PI: Yuri Netto), yielding a S/N similar to that achieved in the combined spectra of Kronos and Krios. However, it is worth mentioning that the most accurate differential study, in terms of abundance precision, is conducted between the components of the binary system due to their similarity.

MAROON-X spectra were reduced using MAROONXDR[3], a publicly available Data Reduction for Astronomy from Gemini Observatory North and South (DRAGONS, Labrie et al. 2019) implementation of the data reduction pipeline, following the standard recipe for echelle spectra (e.g. bias and flat corrections, scattered light correction). The continuum normalization and other operations (such as Doppler correction and spectra combination) were carried out using the Image Reduction and Analysis Facility (IRAF)[4].

3. Stellar parameters and abundance analysis

We determined fundamental stellar parameters, such as effective temperature (T_{eff}), surface gravity (log g), metallicity ([Fe/H]),
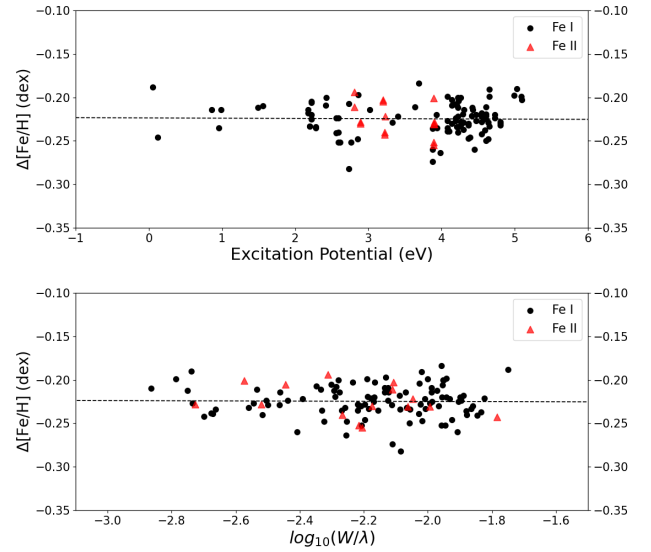

Fig. 1. Differential abundance vs. excitation potential (*upper panel*) and differential abundance vs. reduced EW (*lower panel*) of Krios relative to Kronos. The black dots correspond to Fe I and the red triangles correspond to Fe II.

and microturbulence velocity (v_{turb}), as well as chemical abundances for Kronos and Krios by first measuring the equivalent widths (EWs) of 26 elements, including Fe I and Fe II, using the *splot* task in IRAF[5]. The list of spectral lines, along with significant laboratory data, such as excitation potential, oscillator strengths, and log gf values, were sourced from Liu et al. (2014), Meléndez et al. (2014), and were supplemented with data from Bedell et al. (2014), who carefully selected lines for precise abundance determinations.

Stellar atmospheric parameters were obtained by imposing ionization and excitation balance of the Fe I and Fe II lines. In this method we search for a zero slope when comparing Fe I and Fe II abundances with reduced equivalent width ($EW_r = EW/\lambda$) and excitation potential, respectively. For this purpose, we employed the FUNdamental PARameters programme (FUNDPAR, Saffe et al. 2015, 2018) in its latest version. It uses the MOOG code (Sneden 1973) together with ATLAS12 model atmospheres (Kurucz 1993) to search for the best solution (for more details, see Saffe et al. 2018). In Fig. 1, we present the differential abundances of Fe I (black) and Fe II (red) versus excitation potential (upper panel) and reduced EWs (lower panel) for Krios compared to Kronos.

We employed a full[6] line by line differential technique using the Sun as reference in the first step. In this context, the adopted solar parameters were $T_{\mathrm{eff}} = 5777$ K, log $g = 4.44$ dex, [Fe/H] = 0.00 dex and $v_{\mathrm{turb}} = 1.00$ km s^{-1}. Subsequently, we recalculated v_{turb} by ensuring a zero slope between absolute abundances of Fe I and EW_r, and the value obtained was 1.13 km s^{-1}. The final parameters for Kronos and Krios relative to the Sun are presented in Table 1. The corresponding uncertainities were estimated using the method described in Saffe et al. (2015), which accounts for the individual and mutual co-variances for the error propagation. We applied the same methodology to determine the differential stellar parameters and abundances of Krios, using Kronos as the reference star.

Table 1. Fundamental parameters obtained for Kronos and Krios.

Star	$T_{\rm eff}$ (K)	$\log g$ (dex)	[Fe/H] (dex)	$v_{\rm micro}$ (km s^{-1})	$T_{\rm eff}$ [†] (K)	$\log g$ [★] (dex)
			Our work			
Kronos–Sun	5895 ± 66	4.44 ± 0.06	0.220 ± 0.007	1.18 ± 0.04	5903 ± 51	4.40 ± 0.04
Krios–Sun	5892 ± 52	4.49 ± 0.08	–0.010 ± 0.010	1.18 ± 0.06	5938 ± 40	4.45 ± 0.04
Krios–Kronos	5895 ± 38	4.49 ± 0.05	–0.230 ± 0.005	1.19 ± 0.04	–	–
			Brewer et al. (2016)			
Kronos–Sun	5803 ± 25	4.33 ± 0.03	0.20 ± 0.010	0.85	–	–
Krios–Sun	5878 ± 25	4.43 ± 0.03	0.01 ± 0.010	0.85	–	–

Notes. [†]Photometric effective temperature. [★]Trigonometric $\log g$ obtained from PARAM 1.5.

The resulting parameters for Krios relative to Kronos are also provided in Table 1.

We also derived chemical abundances for 26 elements, other than Fe: Li I, C I, O I, Na I, Mg I, Al I, Si I, S I, Ca I, Sc I, Sc II, Ti I, Ti II, V I, Cr I, Cr II, Mn I, Co I, Ni I, Cu I, Zn I, Y II, Zr II, Ba II, La II, Ce II, Pr II, Nd II, and Eu II. For this purpose we implemented a curve of growth analysis by using the latest version of MOOG (Sneden 1973). In order to account for hyperfine structure (HFS) effects, we employed spectral synthesis for V I, Mn I, Co I, Cu I, Li I, Y II, Sc II, and Eu II, incorporating HFS constants from Kurucz & Bell (1995). We also applied abundance corrections for galactic chemical evolution (GCE) based on the [X/Fe]–age correlation from Bedell et al. (2018) for (Krios–Sun) and (Kronos–Sun), following the methodology detailed by Spina et al. (2016) and Yana Galarza et al. (2016). No GCE correction was made for Krios–Kronos, as it is assumed that they were born from the same molecular cloud. Specifically, we considered non-local thermodynamic equilibrium (NLTE) corrections for Ba II (Korotin et al. 2011), Na I (Shi et al. 2004), and O I (Ramírez et al. 2007). The NLTE correction for Ba II is +0.015 dex for Kronos and 0.00 dex for Krios. For Na I we adopted –0.08 dex for both stars, and for O I we adopted +0.11 dex for Kronos and +0.18 dex for Krios. The differential abundances of all elements, along with their corresponding errors, are detailed in Table 2. It is worth mentioning that extensive NLTE corrections are avilable using an interpolation tool at the MPIA website[7]. This service includes several elements (Mg, Si, and Ca, among others) and also Fe I and Fe II corrections. For example, the O I triplet include hydrogen collisions with cross-sections based on quantum-mechanical calculations (Bergemann et al. 2021). The interpolation tool made use of MAFAGS or MARCS model atmospheres. Considering that our calculation used the ATLAS12 model, a future implementation of FUNDPAR using the MARCS models could take advantage of the mentioned NLTE corrections. The total abundance errors ($\sigma_{\rm TOT}$) were obtained by quadratically adding the observational errors (derived as $\sigma/\sqrt{(n-1)}$) and errors due to uncertainties in fundamental parameters. For those elements with only one line, we adopted for σ the average standard deviation of the other elements.

Using the spectroscopic stellar parameters obtained for both components, we derived new values for stellar masses $M_\star$, radius $R_\star$, and ages $\tau_\star$. To accomplish this, we employed PARAM 1.5[8] from the PAdova and tRieste Stellar Evolution Code (PARSEC) (De Silva et al. 2006; Rodrigues et al. 2014,

Table 2. Differential abundances obtained for Kronos and Krios relative to the Sun and for Krios relative to Kronos.

Species	Kronos–Sun		Krios–Sun		Krios–Kronos	
	[X/Fe]	$\sigma_{\rm TOT}$	[X/Fe]	$\sigma_{\rm TOT}$	[X/Fe]	$\sigma_{\rm TOT}$
C I	–0.295	0.034	–0.070	0.040	0.218	0.029
O I	–0.259	0.079	–0.163	0.062	0.090	0.055
Na I	–0.271	0.046	–0.101	0.031	0.168	0.030
Mg I	0.016	0.067	0.014	0.089	–0.005	0.044
Al I	0.075	0.018	0.051	0.029	–0.028	0.013
Si I	–0.017	0.006	0.016	0.023	0.031	0.016
S I	–0.235	0.032	–0.037	0.026	0.192	0.024
Ca I	0.050	0.026	0.020	0.039	–0.029	0.019
Sc I	0.013	0.054	0.027	0.065	0.014	0.053
Sc II	0.060	0.039	0.011	0.022	–0.059	0.02
Ti I	0.054	0.017	0.017	0.018	–0.036	0.013
Ti II	0.047	0.034	0.037	0.032	–0.014	0.027
V I	0.023	0.032	–0.008	0.035	–0.036	0.023
Cr I	–0.019	0.019	–0.014	0.020	0.007	0.014
Cr II	–0.021	0.028	0.002	0.032	0.021	0.027
Mn I	–0.169	0.081	–0.078	0.073	0.090	0.065
Co I	0.029	0.029	0.008	0.031	–0.025	0.021
Ni I	0.023	0.008	–0.004	0.011	–0.028	0.006
Cu I	–0.251	0.064	–0.070	0.050	0.175	0.045
Zn I	–0.108	0.065	0.041	0.062	0.144	0.052
Y II	–0.083	0.062	–0.037	0.065	0.055	0.052
Zr II	0.051	0.065	0.010	0.062	–0.033	0.052
Ba II	0.256	0.065	0.059	0.062	–0.185	0.052
La II	0.032	0.065	–0.075	0.062	–0.097	0.052
Ce II	–0.067	0.065	–0.118	0.062	–0.041	0.052
Pr II	–0.013	0.065	–0.029	0.062	–0.010	0.052
Nd II	0.196	0.051	0.142	0.067	–0.047	0.052
Eu II	0.144	0.065	0.118	0.062	–0.025	0.052
A(Li) [a]	2.84	0.070	2.28	0.070	–0.56	0.069

Notes. The total error $\sigma_{\rm TOT}$ includes errors due to parameters and observational errors. [a]Absolute abundance of Li.

2017). We specifically utilized the evolutionary tracks from Modules for Experiments in Stellar Astrophysics (MESA; Paxton et al. 2011, 2013, 2015, 2018); the initial data required for the analysis included $T_{\rm eff}$, $\log g$, and [Fe/H], along with the respective 1σ error in all cases. We also included parallaxes from *Gaia* EDR3 (Gaia Collaboration 2021) and photometry from *Tycho*-2 catalogue in V and B bands (Hog et al. 2000). The derived values

---

[7] https://nlte.mpia.de
[8] http://stev.oapd.inaf.it/cgi-bin/param/

are $M_\star = 1.14^{+0.02}_{-0.04}\ M_\odot$, $R_\star = 1.11^{+0.06}_{-0.04}\ R_\odot$, $\tau_\star = 1.95^{+1.68}_{-1.34}$ Gyr for Kronos, and $M_\star = 1.04^{+0.02}_{-0.02}\ M_\odot$, $R_\star = 1.01\ \pm 0.04\ R_\odot$, $\tau_\star = 1.57^{+1.67}_{-1.10}$ Gyr for Krios. In addition, we estimated the ages of the components using trigonometric log g, obtaining as a result $\tau_\star = 2.18 \pm 1.37$ Gyr for Kronos and $\tau_\star = 2.09 \pm 1.50$ Gyr for Krios, which are similar to the previous values within the errors, providing evidence of the true coevality of the system.

4. Results and discussion

The stellar parameters and chemical abundances derived from this work were obtained through the opacity sampling method, incorporating non-solar-scaled opacities (Saffe et al. 2018). When comparing the fundamental atmospheric parameters listed in Table 1 with those obtained from Brewer et al. (2016), we find a good agreement within the errors. However, a notable discrepancy arises when comparing $T_{\rm eff}$ differences between the two components. In our investigation these temperatures exhibit notable similarity, yielding identical temperatures when using Kronos as the reference star. In contrast, Brewer et al. (2016) reports a significant temperature difference between the components. We attribute this discrepancy to the use of higher S/N spectra, the use of different line lists and atmospheric models, and the full line-by-line differential technique employed in our study.

Moreover, it is noteworthy that the atmospheric model utilized in the prior chemical analysis, as indicated by Brewer et al. (2016), employed a fixed microturbulence parameter set at $0.85\ {\rm km\,s^{-1}}$. Nissen & Gustafsson (2018) have cautioned against the potential inaccuracies associated with using a constant value for $v_{\rm turb}$. This caution gains particular significance considering an observed variation of approximately $1.2\ {\rm km\,s^{-1}}$ when analysing stars with effective temperatures ranging between 5000 K and 6500 K (Edvardsson et al. 1993; Ramírez et al. 2013). In our study, we opted not to fix $v_{\rm turb}$; instead, we estimated the value that best fits with the atmosphere model of the components, achieving an optimal agreement between abundances and line intensity.

Additionally, we calculated the photometric temperatures of the two stars using the COLTE code[9], which derives colour-effective temperature relations employing *Gaia* DR3 and 2MASS photometry in the InfraRed Flux Method, and estimating errors from Monte Carlo simulations of each index (Casagrande et al. 2021). The weighted average results can be observed in Table 1. For Kronos there is excellent concordance between spectroscopic and photometric $T_{\rm eff}$, and for Krios the photometric temperature appears marginally higher than the spectroscopic value, although still statistically indistinguishable within the errors. Nevertheless, the spectroscopic estimate exhibits a slightly closer agreement with the photometric value compared to those derived by Brewer et al. (2016).

The significant difference in metallicity found in Oh et al. (2018) of ∼0.20 dex is also reflected in this study, with a difference of 0.230 dex, indicating that Kronos is more metal-rich than Krios. Figure 2 shows the abundance of chemical elements in Krios versus condensation temperature $T_{\rm C}$, considering Kronos as reference. The 50% $T_{\rm C}$ values were taken from Lodders (2003), for a solar composition gas. We calculated the slope considering all elements and considering only the refractories. The weighted results were $-17.43 \pm 2.25\ \times10^{-5}$ dex K^{-1} for all elements and $-23.98 \pm 5.16\ \times10^{-5}$ dex K^{-1} for refractories. Based
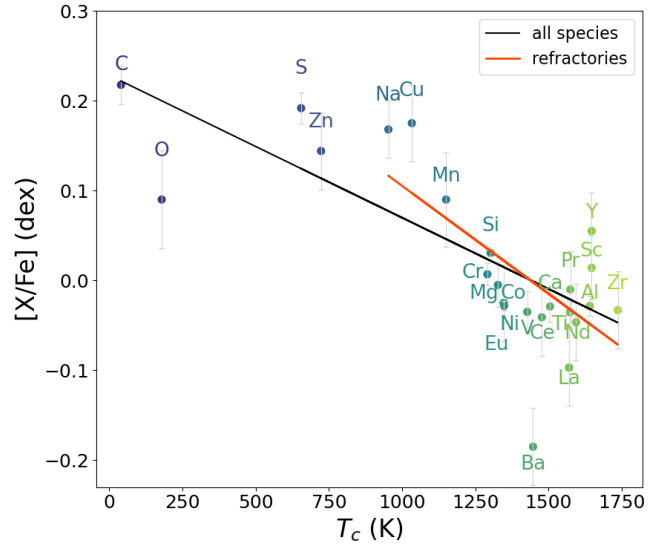
Fig. 2. Differential abundances from Krios–Kronos vs. $T_{\rm C}$. The weighted linear fits to all elements and to refractories are represented as a black and a red line, respectively.

on these findings, a pronounced lack of refractories relative to volatiles in Krios compared to Kronos is evident, with a significance at a 9σ level. Regarding the refractory elements, we can observe that this slope is also significant at a 6σ level.

In view of their results, Oh et al. (2018) explored the possibility that this system formed through binary-single scattering events, where initially unrelated stars undergo an exchange of binary members. The study delves into the rate of exchange scattering, considering factors such as the cross-section and velocity parameters. However, the analysis revealed that this mechanism is unlikely to explain the distinctive abundance patterns observed in such stars. A statistical examination, employing randomly drawn star pairs with similar metallicity characteristics, reinforces this conclusion, highlighting the improbable nature of exchange scattering in accounting for the observed chemical differences within the binary system.

4.1. Li content in Kronos and Krios

The Li abundance was initially calculated for Krios and Kronos using spectral synthesis of the 6707.8 Å line and corrected for NLTE effects using the INSPECT tool (Lind et al. 2012), obtaining $A({\rm Li}) = 2.78 \pm 0.07$ dex for Kronos and $A({\rm Li}) = 2.26 \pm 0.07$ dex for Krios. However, due to an artefact observed around the lithium line, particularly on its left wing, we opted to use spectra from the HIRES database (Programme ID: Y219, PI: Brewer) to redetermine its abundance. After correcting for NLTE effects using the INSPECT tool, we obtained $A({\rm Li})$ values of 2.84 ± 0.07 dex for Kronos and 2.28 ± 0.07 dex for Krios, in good agreement with the values obtained with MAROON-X spectra, within the errors. Consequently, the lithium difference between components is $\Delta({\rm Li}) = 0.56$ dex, slightly greater than the $\Delta({\rm Li}) = 0.50$ dex reported by Oh et al. (2018).

Prior studies of FGK dwarf and subgiant stars revealed a subtle trend between lithium abundance and $T_{\rm eff}$, with $A({\rm Li})$ being higher for hotter stars (Ramírez et al. 2012; Bensby & Lind 2018). Furthermore, Carlos et al. (2019) found a strong correlation between Li depletion and age for a sample of 77 solar-type stars, and a weaker correlation with metallicity and mass, with higher Li depletion for older, more metallic, and less massive
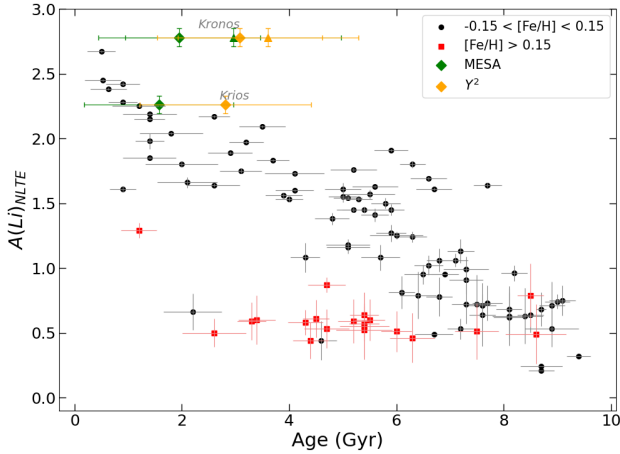
Fig. 3. Lithium abundance vs age for a sample of solar analogues extracted from Martos et al. (2023). The orange diamonds represent Kronos and Krios with ages calculated using Y^2 isochrones, along with their respective metallicities. The orange triangle represents Kronos with a bulk metallicity composition of [Fe/H] = −0.01 dex. Similarly, the green diamonds and triangle represent Kronos and Krios, considering ages calculated with MESA isochrones.

stars, in line with previous studies (e.g. Castro et al. 2009; Carlos et al. 2016).

Recently, Martos et al. (2023) estimated a correlation between Li abundance and both age and [Fe/H] in a sample of 118 solar analogues, using a least-squares method, and found a robust anticorrelation with these parameters. In Fig. 3 of their work, they showed the behaviour of A(Li) with respect to age and [Fe/H]. In Fig. 3, we replicated this distribution by plotting A(Li)$_{NLTE}$ versus age, including those objects with −0.15 < [Fe/H] < 0.15 (black points) and [Fe/H] > 0.15 (red squares). We included Kronos and Krios, shown in the figure with diamonds. Given the significant difference in metallicity between both stars, we also contemplated the hypothesis that the bulk composition of Kronos closely resembled that of Krios, indicated with triangles in the figure. We considered ages computed using MESA isochrones, indicated in green in Fig. 3. Additionally, we incorporated ages calculated through the Yonsei-Yale (Y^2) set of isochrones (Yi et al. 2001; Demarque et al. 2004) and taking into account the influence of alpha enhancement, to maintain consistency with the sample analysed by Martos et al. (2023), resulting in $\tau_\star$ = 3.08 ± 1.54 Gyr and $\tau_\star$ = 2.81 ± 1.60 Gyr for Kronos and Krios, and $\tau_\star$ = 3.61 ± 1.69 Gyr for Kronos considering [Fe/H] = −0.01 dex, represented in the figure in orange. First, we focussed on the MESA set of parameters; it is apparent that Krios has a similar A(Li) to the other stars in the same age group. However, the behaviour of Kronos is quite different from the stars of the same age and metallicity in the sample. It can be observed that, regardless of the primordial metallicity that Kronos may have had, it has more lithium than the rest of the stars in the sample. This phenomenon remains prominent in both cases, whether its primordial metallicity was [Fe/H] = −0.01 dex initially, or considering a bulk metallicity of [Fe/H] = 0.22 dex. Furthermore, these results are also replicated with the set of Y^2 parameters. This suggests that the difference in lithium between the two stars cannot be solely explained by differences in parameters. If this were the case, we would expect Kronos to be defficient in Li compared to Krios, considering Li <1 dex, following the trend of the metal-rich stars in the sample; however, it has Li = 2.78 dex, which is far from this sequence.

Due to the considerable depletion of lithium in stars, which can exceed a factor of 100 at the solar age (e.g. Asplund et al. 2009; Monroe et al. 2013), planet engulfment provides a viable mechanism for significantly increasing the photospheric lithium content in solar-type stars (e.g. Ramírez et al. 2012; Meléndez et al. 2017). Sandquist et al. (2002) showed that planet accretion onto the host star could introduce planet material into the stellar convection zone, thereby modifying surface abundances, especially with respect to lithium.

Meléndez et al. (2017) found an increase in Li in HIP 68468 of approximately 0.6 dex, four times more than expected for a star of its age, attributing this phenomenon to a possible planet ingestion. In a similar work, Galarza et al. (2021) analysed the binary system HIP 71726–HIP 71737. Their analysis revealed a metallicity difference of Δ(Fe/H) ∼ 0.11 dex and a lithium disparity of ∼1.03 dex between the components. The authors concluded that an engulfment event involving ∼9.8 $M_\oplus$ of rocky material could account for these observed differences. Spina et al. (2021) analysed the chemical composition of 107 binary systems composed of solar-type stars, finding that those stars with higher [Fe/H] than their companions also exhibited an increase in Li abundance, linking both results to planetary ingestion by these enriched objects. They determined that engulfment events occur with a probability of 20–35%. Nonetheless, Behmard et al. (2023) claim that the use of an inhomogeneous sample, the omission of an analysis of abundances with T_C, and the fact that some binaries in the sample did not qualify as twins could significantly affect the high rates of engulfment found by Spina et al. (2021). Instead, they conducted a more detailed analysis of 36 planet-hosting binaries, of which only 11 systems were considered twins, aiming to detect potential engulfment events. This exploration revealed that engulfment events are rare, with a rate of ∼2.9%. Notably, the study emphasizes that only the Krios–Kronos binary could have experienced a genuine engulfment event.

4.2. Searching for planets around Kronos and Krios

To date, there have been no planets detected in orbit around Kronos and Krios. Therefore, we conducted a detailed photometric analysis with the aim of revealing potential planetary bodies that could offer valuable insights to the planet formation scenarios expounded in the subsequent sections.

Both stars were observed by the Transiting Exoplanet Survey Satellite mission (TESS; Ricker et al. 2015) in sectors 17, 18, and 24 (from October 8 to November 27, 2019, and from April 16 to May 12, 2020) with a 30-min cadence and in sectors 57 and 58 (September 30–November 26, 2022) with a cadence of 200 s. The analysis of these data products, available in target pixel file (TPF) format, was carried out with the tools provided by the Lightkurve Python package (Lightkurve Collaboration 2018). Given that both stars are sufficiently separated in the TESS field, we were able to analyse the TPF files of Kronos and Krios independently. We performed single-aperture photometry on the images, choosing as optimal aperture the one centred on the target that allowed all the possible flux to be collected from the star, but that minimized the sky contribution. The 30-min and 200-s cadence light curves were treated separately. For both modes, a median filter was applied to remove the systematics in the resulting light curves. We were not able to eliminate the strong systematics introduced by the changes in the Earth-Moon orientation and distance in sector 24 and, hence, these data were not used in the further analysis.
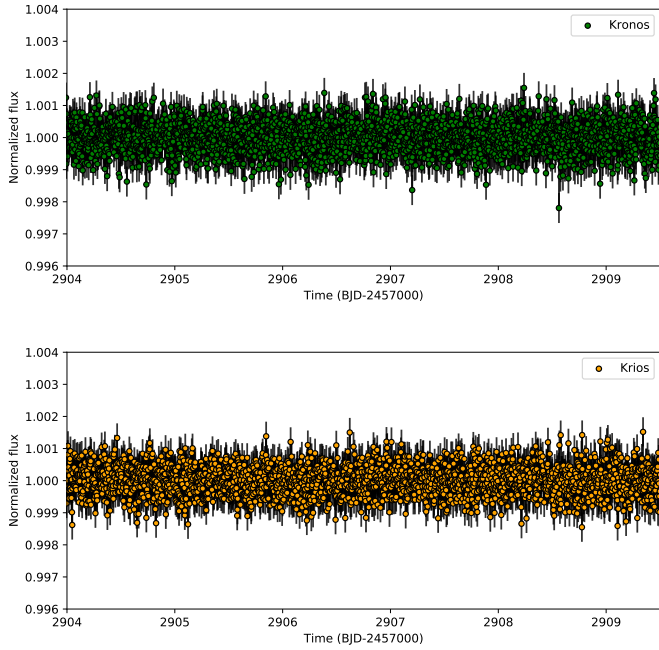
Fig. 4. Portion of the detrended TESS light curves of Kronos (*top*) and Krios (*bottom*) considering the 200-s cadence data of sector 58.

To look for signs of additional stellar and/or planetary companions around Kronos and Krios, we ran the Transit Least Squares code (TLS; Hippke & Heller 2019) on the detrended light curves of each component separately (Fig. 4). No transit or eclipse-like signal that could suggest the presence of a transiting planet or an eclipsing stellar companion was detected in the 30-min or in the 200-s cadence of the two stars. Additionally, a detailed by-eye inspection of the TESS photometry revealed that the stars show no signs of periodic modulation or sporadic events, such as flares, which indicates that they are not photometrically active objects. Here, it is important to caution that the present conclusion about the periodic photometric variability is based only on visual scrutiny of the data. In order to obtain a more reliable and confident result, we should run on the TESS light curves of Kronos and Krios a tool specifically designed to detect periodic modulations in time series, such as the Lomb–Scargle periodogram (Lomb 1976; Scargle 1982) or the auto-correlation function (McQuillan et al. 2013). However, conducting such an analysis is beyond the scope of this paper.

4.3. Atomic diffusion

The atomic diffusion process includes effects such as gravitational settling, thermal and chemical diffusion, and radiative acceleration (e.g. Dotter et al. 2017; Liu et al. 2021). It primarily operates in the radiative zones of the stars, pushing certain elements and altering its surface abundances, depending on the particular species and the evolutionary state of the star. In the case of substantial differences in the spectroscopic parameters of stars (T_{eff} or $\log g$) forming a binary system, this process could potentially explain a disparity in metallicity between the components since their abundances may have been affected differently as they evolve. Liu et al. (2021) found that, for four of the seven studied pairs with differences in $\log g > 0.05$ dex, their discrepancies in [Fe/H] could be attributed to atomic diffusion rather than planetary formation.
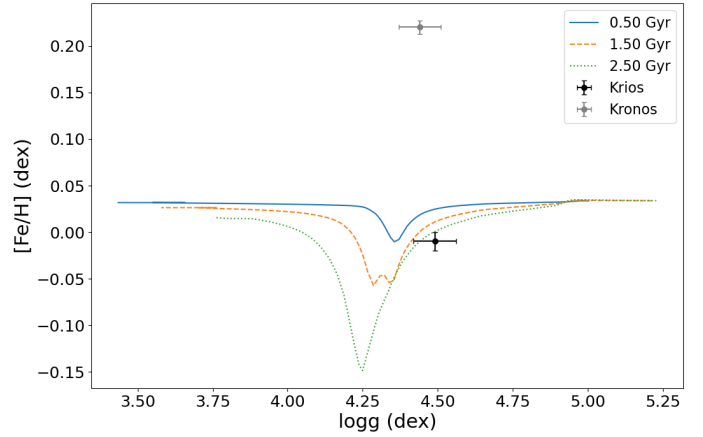

Fig. 5. Set of isochrones for an age range of 0.5–2.5 Gyr. Krios is plotted in black and Kronos in grey. The vertical and horizontal bars correspond to σ[Fe/H] and $\sigma \log g$, respectively.

In the present work, Kronos and Krios exhibit a $\log g$ difference of approximately 0.05 dex. In consequence, we investigate whether the observed difference in metallicity between the components could be attributed to a diffusion process. To address this, we used the MESA Isochrones and Stellar Tracks (MIST[10]; Choi et al. 2016), which facilitates the derivation of stellar evolutionary models that integrate the influences of atomic diffusion and overshoot mixing, and also employed solar abundances from Asplund et al. (2009). We generated a set of isochrones covering the age range of both stars; the results are depicted in Fig. 5. From the figure, it is evident that Krios follows an evolutionary model consistent, within the errors, with the age calculated from PARAM ($\tau_\star \approx 1.57$ Gyr). With Kronos exhibiting a lower $\log g$ than Krios, the metallicity of Kronos would be expected to be lower if diffusion was predominant in explaining the anomalies found. However, as depicted in Fig. 5, Kronos exhibits a significantly higher metallicity than Krios. Based on this result, while this effect cannot be completely ruled out, we can consider that it is not the primary factor responsible for the pronounced difference in metallicity found in the binary system. There must be an additional mechanism to account for these discrepancies.

4.4. Primordial chemical differences between components

Binary systems are ideal laboratories for testing a number of scenarios that have been proposed to explain the origin of chemical signatures. This is attributed to the shared origin of the two stars within the same molecular cloud, assuming that their primordial chemical composition should be similar and diminishing the factor of GCE.

Taking into account the substantial difference in metallicity between Kronos and Krios, having a projected separation of approximately 11 277 au, Oh et al. (2018) explored the probability of their coincidental pairing. Using the *Gaia* Universe Mock Simulation (Robin et al. 2012) and the Besançon Galaxy model (Robin et al. 2003), they looked for chance pairs within 200 parsec of the Sun. From a sample of 119 259 solar-mass primary stars, they found only one pair with $\Delta v_r < 2\,\mathrm{km\,s^{-1}}$, which naturally suggests a physical association between the Kronos and Krios system rather than a chance pairing. We further calculated the Δv_{3D} of the binary system. For this purpose, we utilized the space velocities of each component from the *Gaia* DR3 dataset

---

[10] https://waps.cfa.harvard.edu/MIST/index.html

(Gaia Collaboration 2021) using the GALA code (Price-Whelan 2017). The Δv_{3D} is estimated at $0.55\,\mathrm{km\,s^{-1}}$, which is below the $2\,\mathrm{km\,s^{-1}}$ limit required to ensure the continuity of a binary system (Kamdar et al. 2019b).

Ramírez et al. (2019) examined a sample of 12 binary systems with twin stars, and found a modest correlation between the absolute difference in metallicity among the components and their separation. They found increased metallicity discrepancies with expanding separations between the binary system components. Additionally, Andrews et al. (2019) investigated chemical homogeneity in 24 binary systems with similar components, finding consistency in their abundances at a level of 0.1 dex. Furthermore, they generated a set of random pairs from these systems, and in this case, consistency was observed at a level of 0.3–0.4 dex. Following this line, Nelson et al. (2021) analysed 33 comoving pairs of F and G dwarfs and found that those comoving systems spanning separations from $\sim 2 \times 10^5$ au to 2×10^7 au exhibit greater homogeneity (Δ[Fe/H] = 0.09 dex) than those that are randomly paired (Δ[Fe/H] = 0.23 dex).

Assuming that the two stars indeed constitute a coeval and conatal system, and considering the results presented by Nelson et al. (2021), it suggests that the difference in metallicity found in the binary system cannot be solely explained by their separation distance, suggesting the existence of some other factor to account for this significant discrepancy.

4.5. Planet formation scenarios

4.5.1. Rocky planet formation

The average abundance calculated for refractory and volatile elements for Krios-Kronos are -0.24 ± 0.01 dex and -0.03 ± 0.03 dex, respectively. These results, along with the trend observed in Fig. 2, indicate an overabundance of refractories in Kronos compared to Krios. Moreover, as seen in Sect. 4.1, there is an excess of Li in Kronos of Δ(Li) = 0.56 dex, which cannot be solely explained by differences in the parameters of the components.

Among the possible scenarios that could explain this result, we firstly consider the hypothesis presented by Meléndez et al. (2009). They suggested that the lack of refractories in the Sun may be attributed to the formation of terrestrial planets and planetesimals around it, which primarily accreted refractory material for this purpose (e.g. Saffe et al. 2016; Yana Galarza et al. 2016; Liu et al. 2020). The fact that Krios exhibits a deficiency in refractories could potentially result from a protoplanetary disc sequestering refractory material, possibly for the subsequent formation of rocky planets around the star. To date, as we present in Sect. 4.2, no planets have been detected transiting either component of the binary system. While current evidence does not provide strong support for this model, it would be intriguing to conduct a radial velocity study to search for possible anomalies that could indicate the presence of a planet.

Another plausible factor that may account for the disparity in metallicity and the trend with T_C among the binary system components is the potential presence of a debris disc encircling Krios, similar to what was observed in the $\zeta^1 - \zeta^2$ Ret system (Saffe et al. 2016). Debris disc detection primarily relies on identifying infrared (IR) excess emissions originating from circumstellar dust. These dust particles have lifespans shorter than those of stellar systems, reinforcing the hypothesis that these discs experience continuous replenishment through ongoing collisions with substantial celestial bodies (e.g. Wyatt 2008).

To investigate the potential presence of an IR excess in this binary system, we employed the VOSA[11] platform, obtaining the energy distribution for both system components using photometric observations from the SDSS, JPAS, *Tycho*, JPLUS, Johnson, WISE, 2MASS, and *Gaia*3 filters. The analysis did not reveal any IR excess in either component, discouraging the possibility that the observed differences in metallicity and the T_C trend in this system are linked to the presence of a debris disc around Krios.

4.5.2. Dust trapping

The model proposed by Booth & Owen (2020) suggests that the lack of refractories in one of the stars could be due to the formation of a massive gas giant planet that created a gas gap in the protoplanetary disc. This gap transforms into an outer pressure trap beyond the orbit of the planet, mainly sequestering dust from the disc. This mechanism could reveal a disparity between refractory and volatile elements in the hosting star. The recent study by Hühn & Bitsch (2023) refines the understanding of this planetary formation scenario, exploring how the origin of a planet influences the material accreted onto the convective envelope.

If we consider this scenario as plausible, Krios should have a Jupiter-sized planet in orbit, which, according to this model, would create traps allowing the accretion of volatiles while inhibiting the accretion of refractories. If this were the case, it could potentially account for the abundance pattern observed in Fig. 2. The absence of detected planets to date does not provide conclusive evidence to entirely rule out this hypothesis.

4.5.3. Planetary ingestion

Another important scenario to consider is the engulfment hypothesis (e.g. Saffe et al. 2017; Galarza et al. 2021; Jofré et al. 2021; Flores et al. 2024). Spina et al. (2021) suggested that two conditions must be met for the observed anomalies to be attributed to the engulfment of a planet. Firstly, there should be an excess of refractory elements compared to volatiles in one of the stars in the pair, indicating the accretion of rocky material by that object. Secondly, it should also exhibit an excess of Li compared to its companion. This latter characteristic becomes particularly significant when engulfment occurs at an advanced age of the star because, by that time, it would have already burned most of the Li in its atmosphere, and therefore the accretion of new refractory material would leave a substantial and detectable imprint when comparing the A(Li) of the two components.

When comparing our findings with the hypotheses presented in the work of Spina et al. (2021), the scenario of engulfment becomes a plausible consideration. This implies that Kronos might have undergone the accretion of one or more planets at an advanced age, leaving distinctive lithium content marks and introducing refractory elements into the atmosphere of the star. To determine how much terrestrial mass Kronos would need to have accreted to achieve these values, we employed the TERRA code[12] (Galarza et al. 2016). Our estimations reveal a convection envelope mass of M_{cz} = 0.017 $M_\odot$ for Kronos, with approximately $\sim 27.8\ M_\oplus$ of rocky material considered necessary to replicate the observed trend illustrated in Fig. 2. This includes a combination of 19.9 $M_\oplus$ of terrestrial material and 7.9 $M_\oplus$ of meteoritic material. This remarkable magnitude of ingested

---

[11] http://svo2.cab.inta-csic.es/theory/vosa/index.php
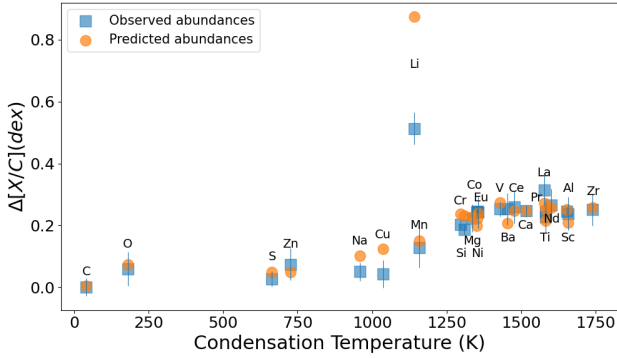[12] https://github.com/ramstojh/terra

Fig. 6. Observed and predicted abundances of Kronos–Krios vs. T_C (blue squares and orange dots, respectively), considering that Kronos ingested $\sim$27.8 $M_\oplus$.

material represents one of the largest estimated to date in twin components, underscoring the significance of the results. Furthermore, recent research conducted by Armstrong et al. (2020) provides compelling evidence of the existence of TOI849-b, a planet with a core mass of 39.1 $M_\oplus$. This discovery not only reinforces the plausibility of our findings, but also highlights the prevalence of planetary bodies with masses comparable to or even greater than the values found in our study within exoplanetary systems.

Figure 6 depicts the observed model and the model adjusted by TERRA, taking into account the ingestion of $\sim$27.8 $M_\oplus$. A good agreement between the two models is evident, except for Li, which is overestimated by $\sim$0.36 dex. We caution that TERRA models engulfment as if it had occurred at the present time. Hence, the excess of Li found in the predicted model suggests that the engulfment likely occurred in the past. The mass of the convective envelope plays a significant role; therefore, knowing this value at the time of accretion would contribute to improving the model. Nonetheless, the simulation predicted by TERRA can be considered a solid first approximation.

Behmard et al. (2023) employed a sample of 36 stellar systems to quantify the duration a chemical signature could remain observable in the stellar photosphere due to the ingestion of a planet and its associated strength. They simulated pollution resulting from the engulfment of a 10 $M_\oplus$ planet and found that stars with masses ranging between 1.1 and 1.2 $M_\odot$ exhibited the highest and most enduring chemical signature, maintaining values greater than 0.05 dex for approximately 2 Gyr. They also conducted an analysis considering the ingestion of a 50 $M_\oplus$ planet, where stars with masses between 0.7 and 1.2 $M_\odot$ displayed signatures exceeding 0.05 dex for a duration spanning 3–8 Gyr. Taking into account the age and mass of Kronos, these findings lead us to consider that the chemical differences observed in this star when compared to Krios, may have originated from a potential engulfment of rocky material.

The Kozai migration (Kozai 1962) has been proposed to explain this phenomenon in other binary systems, wherein a giant planet orbiting one of the stars may experience orbital decay due to a combination of perturbations caused by the other star in the system that leads to an increase in the eccentricity of the planetary orbit, accompanied by tidal friction that brings the planet closer to the host star, ultimately resulting in the ingestion of the surrounding rocky material and potentially the planet itself (Wu et al. 2003; Takeda et al. 2008; Borkovits et al. 2011; Mustill et al. 2015; Petrovich 2015; Church et al. 2020). In this context, we should assume that Kronos initialy formed a giant gas planet

as well and possibly rocky material. Then the migration of this hypothetical planet triggered the accretion of refractory material, either from the inner regions of the planetary system or from the giant planet's core itself, resulting in the observed refractory excess (as shown in Fig. 2). Some similar migration scenarios have been invoked in the literature for other binary systems (e.g. Neveu-VanMalle et al. 2014; Teske et al. 2015; Saffe et al. 2017; Jofré et al. 2021; Flores et al. 2024).

5. Conclusions

We performed a high-precision differential abundance analysis of the binary system Krios and Kronos with the aim of exploring different scenarios that could explain the particularly high [Fe/H] disparity found in Oh et al. (2018). To achieve this, we took advantage of high-resolution spectra ($S/N\sim$420) obtained from MAROON-X. We calculated the fundamental atmospheric parameters ($T_{\rm eff}$, log g, [Fe/H], $v_{\rm turb}$) for the two stars, for the first time making use of the non-solar-scaled method and using the Sun as reference, and recalculated parameters of Krios using Kronos as reference. We also measured chemical abundances for 27 elements through equivalent widths and spectral synthesis, subsequently analysing their relation with the T_C. We found high similarity in the fundamental parameters of the two components and confirmed the existing difference in metallicity between them, with Kronos having a metallicity $\sim$0.230 dex higher than Krios. This substantial disparity suggests that previous chemical tagging works may not have successfully recovered their shared origin (e.g. De Silva et al. 2006; Bovy 2016; Liu et al. 2016; Casamiquela et al. 2020, 2021).

In addition to these results, a significant difference in Li abundance between the components was also found, with Kronos being 0.56 dex more abundant in Li than Krios. When comparing the abundances of (Krios-Kronos) versus T_C, we observed a pronounced trend relative to T_C, a behaviour that is repeated when considering only refractory elements. From these results, we primarily deduce an excess of refractories in Kronos compared to Krios.

We conducted a comprehensive single-aperture photometry analysis using TESS data and the TLS code to investigate potential planets orbiting either of the stars. No transits or eclipses of potential planets orbiting any of the components were detected, and there were no indications of stellar activity. While no evidence of transiting planets around Kronos and Krios was found, it should be noted that planetary-mass bodies that do not transit may still exist in the system. Additionally, it would be compelling to perform an analysis of the radial velocity variations of both components to shed light to this hypothesis.

Different scenarios were considered to explain the results obtained. We introduced, for the first time, an atomic diffusion analysis in this system, given the 0.05 dex difference in log g found between components, the limit considered by Liu et al. (2021) beyond which this phenomenon could affect the metallicity of the components. However, the characteristics of Kronos differ significantly from what was anticipated by its evolutionary model, suggesting that this scenario may not entirely account for the wide difference in metallicity.

We also examined the potential that this difference had a primordial origin, considering the projected separation existing between the stars ($\sim$11 277 au). Following the approach of Nelson et al. (2021), given that comoving pairs exhibit differences in metallicity of Δ[Fe/H] $\sim$ 0.09 dex, and taking into account that both stars probably formed from the same gas and

dust cloud (Oh et al. 2018), we suggest that the difference in metallicity between the components cannot be solely associated with primordial differences; this implies the presence of an additional factor influencing this substantial disparity.

Planet formation scenarios were also investigated. The T_C trend found in Fig. 2, if interpreted as a deficiency of refractories in Krios, could have its origin in the formation of rocky planets (not yet detected), as proposed by Meléndez et al. (2009). We also analysed the IR excess, searching for a possible dust disc in Krios that could be generating the observed effect, with no positive results. Additionally, the scenario proposed by Booth & Owen (2020) was analysed in this binary system for the first time, assuming the presence of a hypothetical Jupiter-sized planet orbiting Krios, in which case pressure traps that sequester refractory elements could generate the observed pattern. However, additional photometric and spectroscopic data are necessary to conduct a more detailed search for planets around Krios, and to shed light on this hypotheses.

The last scenario analysed was planetary engulfment, a phenomenon whose characteristics closely match the results found in Kronos, both in the excess of [Fe/H] and the excess of Li compared to Krios (Spina et al. 2021). Regarding this hypothesis, we calculated the amount of rocky material Kronos would have ingested to achieve this difference through the TERRA code, resulting in ~27.8 $M_\oplus$.

In conclusion, while the evidence may seem to favour the engulfment hypothesis, it is crucial to acknowledge the inherent complexities and uncertainties associated with each scenario. Therefore, further investigation and exploration are imperative in order to achieve a more comprehensive understanding of the chemical anomalies and dynamics within this binary system.

References

Adibekyan, V., González Hernández, J., Delgado-Mena E., et al. 2014, A&A, 564, A15

Andrews, J., Chanamé, J., Agüeros, M. 2018, MNRAS, 473, 5393

Andrews, J., Anguiano, B., Chanamé, J., et al. 2019, ApJ, 871, 42

Armstrong, D. J., Lopez, T. A., Adibekyan, V., et al. 2020, Nature, 583, 39

Asplund, M., Grevesse, N., Sauval, A., & Scott, P. 2009, ARA&A, 47, 481

Bedell, M., Meléndez J., Bean J. L., et al. 2014, ApJ, 795, 23

Bedell, M., Bean, J. L., Meléndez, J., et al. 2018, ApJ, 865, 68

Behmard, A., Dai, F., Brewer, J., et al. 2023, MNRAS, 521, 2969

Bensby, T., & Lind, K. 2018, A&A, 615, A151

Bergemann, M., Hoppe, R., Semenova, E., et al. 2021, MNRAS, 508, 2236

Booth, R., & Owen, J. 2020, MNRAS, 493, 5079

Borkovits, T., Csizmadia, S., Forgács-Dajka, E., & Hegedüs, T. 2011, A&A, 528, A53

Bovy, J. 2016, ApJ, 817, 49

Brewer, J., Fischer, D., Valenti, J., & Piskunov, N. 2016, ApJSS, 225, 32

Carlos, M., Nissen, P. E., Meléndez, J. 2016, A&A, 587, A100

Carlos, M., Meléndez, J., Spina, L., et al. 2019, MNRAS, 485, 4052

Casagrande, L., Lin, J., Rains, A. D., et al. 2021, MNRAS, 507, 2684

Casamiquela, L., Tarricq, Y., Soubiran, C., et al. 2020, A&A, 635, A8

Casamiquela, L., Castro-Ginard, A., Anders, F., Sourbiran, C. 2021, A&A, 654, A151

Castro, M., Vauclair, S., Richard, O., & Santos, N. C. 2009, A&A, 494, 663

Choi, J., Dotter, A., Conroy, C., et al. 2016, ApJ, 823, 102

Church, R. P., Mustill, A. J., & Liu F. 2020, MNRAS, 491, 2391

De Silva, G. M., Sneden, C., Paulson, D., et al. 2006, AJ, 131, 455

De Silva, G. M., Freeman, K. C., Bland-Hawthorn, J., et al. 2015, MNRAS, 449, 2604

Demarque, P., Woo, J.-H., Kim, Y.-C., & Yi, S. K. 2004, ApJS, 155, 667

Dotter, A., Conroy, C., Cargile, P., & Asplund, M. 2017, ApJ, 840, 99

Edvardsson, B., Andersen, J., Gustafsson, B., et al.1993, A&A, 275, 101

Flores, M., Galarza, J., Yana, Miquelarena, P., et al. 2024, MNRAS, 527, 10016

Freeman, K., & Bland-Hawthorn, J. 2002, ARA&A, 40, 487

Gaia Collaboration (Brown, A. G. A., et al.) 2021, A&A, 649, A1

Galarza, J. Y., Meléndez, J., & Cohen, J. G. 2016, A&A, 589, A65

Galarza, J. Y., López-Valdivia, R., Meléndez, J., & Lorenzo-Oliveira, D. 2021, ApJ, 922, 129

Gilmore, G., Randich, S., Asplund, M., et al. 2012, Messenger, 147, 25

Gonzalez, G. 1997, MNRAS, 285, 403

González Hernández, J., Delgado Mena, E., Sousa, S. G., et al. 2013, A&A, 552, A6

Hawkins, K., Lucey, M., Yuan-Sen, T., et al. 2020, MNRAS, 492, 1164

Hippke, M., & Heller, R. 2019, A&A, 623, A39

Hog, E., Fabricius, C., Makarov, V. V., et al. 2000, A&A, 355, L27

Hühn, L.-A., & Bitsch, B. 2023, A&A, 676, A87

Jofré, E., Petrucci, R., Gómez Maqueo Chew, Y., et al. 2021, AJ, 162, 291

Kamdar, H., Conroy, C., Ting, Y.-S., et al. 2019a, ApJ, 884, L42

Kamdar, H., Conroy, C., Ting, Y.-S., et al. 2019b, ApJ, 884, 173

Korotin, S., Mishenina, T., Gorbaneva, T., & Soubiran, C. 2011, MNRAS, 415, 2093

Kozai, Y. 1962, AJ, 67, 591

Kunimoto, M., Guillot, T., Ida, S., & Takeuchi, T. 2018, A&A, 618, A132

Kurucz, R. L. 1993, ATLAS9 Stellar Atmosphere Programs and 2 km/s grid, Kurucz CD-ROM 13 (Cambridge, MA: Smithsonian Astrophysical Obs.)

Kurucz, R., & Bell, B. 1995, Atomic Line Data, eds. R. L. Kurucz & B. Bell, Kurucz CD-ROM No. 23 (Cambridge), 23

Labrie, K., Anderson, K., Cárdenes, R., et al. 2019, ASP Conf. Ser., 523, 321

Lightkurve Collaboration (Cardoso, J. V. d. M., et al.) 2018, Lightkurve: Kepler and TESS time series analysis in Python, Astrophysics Source Code Library [record ascl:1812.013]

Lind, K., Bergemann, M., & Asplund, M. 2012, MNRAS, 427, 50

Liu, F., Asplund, M., Ramirez, I., et al. 2014, MNRAS, 442, L51

Liu, F., Yong, D., Asplund, M., et al. 2016, MNRAS, 457, 3934

Liu, F., Yong, D., Asplund, M., et al. 2018, A&A, 614, A138

Liu, F., Yong, D., Asplund, M., et al. 2020, MNRAS, 495, 3961

Liu, F., Bitsch, B., Asplund, M., et al. 2021, MNRAS, 508, 1227

Lodders, K. 2003, AJ, 591, 1220

Lomb, N. R. 1976, Ap&SS, 39, 447

Majewski, S. R., Schiavon, R. P., Frinchaboy, P. M., et al. 2017, AJ, 154, 94

Martos, G., Meléndez, J., Rathsam, A., & Carvalho Silva, G. 2019, MNRAS, 485, 4052

McQuillan, A., Aigrain, S., & Mazeh, T. 2013, MNRAS, 432, 1203

Meléndez, J., Asplund, M., Gustafsson, B., & Yong, D. 2009, ApJ, 704, L66

Meléndez, J., Ramírez, I., Karakas, A. I., et al. 2014, ApJ, 791, 14

Meléndez, J., Bedell, M., Bean, J. L., et al. 2017, A&A, 597, A34

Michalik, D., Lindegren, L., Hobbs, D. 2015, A&A, 574, A115

Monroe, TalaWanda R., Meléndez, J., Ramírez, I., et al. 2013, ApJ, 774, L32

Mustill, A. J., Davies, M. B., Johansen, A. 2015, ApJ, 808, 14

Nelson, T., Ting, Y. S., Hawkins, K., et al. 2021, ApJ, 921, 118

Neveu-VanMalle, M., Queloz, D., Anderson, D. R., et al. 2014, A&A, 572, A49

Nissen, P. E. 2015, A&A, 579, A52

Nissen, P. E., & Gustafsson, B. 2018, A&ARv, 26, 6

Oh, S., Price-Whelan, A., Brewer, J., et al. 2018, AJ, 854, 138

Önehag, A., Korn, A., Gustafsson, B., et al. 2011, A&A, 528, A85

Paxton, B., Bildsten, L., Dotter, A., et al. 2011, ApJS, 192, 3

Paxton, B., Cantiello, M., Arras, P., et al. 2013, ApJS, 208, 4

Paxton, B., Marchant, P., Schwab, J., et al. 2015, ApJS, 220, 15

Paxton, B., Schwab, J., Bauer, Evan B., et al. 2018, ApJS, 234, 34

Petrovich, C. 2015, ApJ, 799, 27

Price-Whelan, A. M. 2017, J. Open Source Softw., 1277, 2

Ramírez, I., Allende Prieto, C., & Lambert, D. 2007, A&A, 465, 271
Ramírez, I., Fish, J. R., Lambert, D. L., & Allende Prieto, C. 2012, ApJ, 756, 46
Ramírez, I., Allende Prieto, C., & Lambert, D. L. 2013, ApJ, 764, 78
Ramírez, I., Khanal, S., Lichon, S., et al. 2019, MNRAS, 490, 2448
Randich, S., Gilmore, G., Gaia-ESO Consortium 2013, Messenger, 154, 47
Ricker, G. R., Winn, J. N., Vanderspek, R., et al. 2015, J. Astron. Telesc. Instrum. Syst., 1, 014003
Robin, A. C., Reylé, C., Derrière, S., & Picaud, S. 2003, A&A, 409, 523
Robin, A. C., Luri, X., Reylé, C., et al. 2012, A&A, 543, A100
Rodrigues, T. S., Girardi, L., Miglio, A., et al. 2014, MNRAS, 445, 2758
Rodrigues, T. S., Bossini, D., Miglio, A., et al. 2017, MNRAS 467, 1433
Saffe, C., Flores, M., & Buccino, A. 2015, A&A, 582, A17
Saffe, C., Flores, M., Jaque Arancibia, M., et al. 2016, A&A, 588, A81
Saffe, C., Jofré, E., Martioli, E., et al. 2017, A&A, 604, A4
Saffe, C., Flores, M., Miquelarena, P., et al. 2018, A&A, 620, A54
Saffe, C., Jofré, E., Miquelarena, P., et al. 2019, A&A, 625, A39
Saffe, C., Miquelarena, P., Alacoria, J., et al. 2024, A&A, 682, L23
Sandquist, E. L., Dokter, J. J., Lin, D. N. C., & Mardling, R. A. 2002, ApJ, 572, 1012
Scargle, J. D. 1982, ApJ, 263, 835
Schuler, S., Cunha, K., Smith, V., et al. 2011, ApJ, 737, L32
Shi, J. R., Gehren, T., & Zhao, G. 2004, A&A, 423, 683
Sneden, C. 1973, ApJ, 184, 839
Souto, D., Cunha, K., Smith, V. V., et al. 2018, ApJ, 857, 14
Souto, D., Allende Prieto, C., Cunha, K., et al. 2019, ApJ, 874, 97
Spina, L., Meléndez, J., & Ramírez, I. 2016, A&A, 585, A152
Spina, L., Sharma, P., Meléndez, J., et al. 2021, Nat. Astron., 5, 1163
Takeda, G., Kita, R., & Rasio, F. A. 2008, IAU Symp., 253, 181
Théado, S., Vauclair, S. 2012, ApJ, 744, 123
Teske, J. K. , Ghezzi, L., Cunha, K. et al., 2015, ApJ, 801, L10
Teske, J., Khanal, S., & Ramírez, I. 2016, ApJ, 819, 19
Tucci Maia, M., Meléndez, J., Lorenzo-Oliveira, D., Spina, L., & Jofre, P. 2019, A&A, 628, A126
Wu, Y., & Murray, N. 2003, ApJ, 589, 605
Wyatt, M. 2008, ARA&A, 46, 339
Yana Galarza, J., Meléndez, J., Ramírez, I., et al. A&A, 589, A17
Yi, S., Demarque, P., Kim, Y.-C., et al. 2001, ApJS, 136, 417